Hindawi
International Journal of Aerospace Engineering
Volume 2022, Article ID 9299470, 19 pages
https://doi.org/10.1155/2022/9299470

Research Article

Active Flow Control of Helicopter Rotor Based on Coflow Jet

Jiaqi Liu,[1,2] **Rongqian Chen**,[1] **Qiaochu Song**,[1] **Yancheng You**,[1] **and Zheyu Shi**[3]

[1]*School of Aerospace Engineering, Xiamen University, Xiamen 361005, China*
[2]*National Key Laboratory of Science and Technology on Aerodynamic Design and Research, Northwestern Polytechnical University, Xi'an 710072, China*
[3]*Rotor Aerodynamics Key Laboratory, China Aerodynamics Research and Development Center, Mianyang 621000, China*

Correspondence should be addressed to Rongqian Chen; rqchen@xmu.edu.cn

Received 11 February 2022; Revised 14 April 2022; Accepted 12 May 2022; Published 6 June 2022

Academic Editor: Teng Wu

When a helicopter rotor undergoes flow separation, the drag of the rotor increases substantially, as does the power demand, which seriously affects the aerodynamic performance and flight safety of the helicopter. Therefore, it is crucial to research how to suppress the flow separation of rotor blades. An active control technique based on a coflow jet (CFJ) at the rotor blade tip was employed in this study to suppress the flow separation over the rotor. The mechanisms and behavior were investigated. The rotor flow field was numerically simulated by solving the Reynolds-averaged Navier–Stokes equations with the finite volume method. The turbulence model was $k-\omega$ SST, and the rotor motion was simulated using the overset mesh technique. After applying CFJ control, the airflow from the injection slot at the leading edge of the rotor increased the energy of the mainstream in the near-wall area, which enhanced its ability to resist the adverse pressure gradient. A flow separation was effectively suppressed, both on the advancing and retreating sides, which improved the aerodynamic performance of the rotor. During the whole rotation period, the thrust coefficient of the rotor increased by up to 5.6%, the moment coefficient decreased by as much as 26.8%, and the equivalent lift-to-drag ratio increased by up to 44.0%. Moreover, the effects of the CFJ parameters on the flow separation suppression of the rotor are researched. These results may provide a foundation for the development of aerodynamic performance improvement for helicopter rotor based on a CFJ.

1. Introduction

A helicopter is a kind of aircraft with the capability for vertical take-off and landing and for hovering. Helicopters not only have good maneuverability but also have a larger flight envelope than other aircraft. Therefore, helicopters are widely used for military and civil applications. When a helicopter flies forward at high speed, the speed of a blade on the advancing side is greater than that of a blade on the backward side due to the superimposition of the rotation speed of the rotor and the forward-flight speed of the helicopter. The advancing blade is prone to shock waves in transonic states, which trigger the occurrence of shock wave/boundary layer interference. This causes the flow to separate from the blade surface which negatively affect the rotor's aerodynamic performance. In contrast, the retreating blade has a high angle of attack (AoA). It often undergoes large-scale flow separation, which causes an unsteady dynamic stall [1–3]. These phenomena lead to a dramatic increase in drag and a significant increase in power demand, which seriously affect the aerodynamic performance of the helicopter and restrict any increase in the forward-flight speed. Hence, it is of great significance to research the flow separation suppression of helicopter rotors.

There are two categories of control method for preventing a flow separation: passive control and active control. Passive control methods for suppressing the shock-induced flow separation of an advancing blade mainly include optimizing the shape of the blade tip, such as the backward sweep, forward sweep, and shape of the curves [4–6], to decompose the flow velocity and delay the shock waves. In addition, Doerffer et al. [7, 8] proposed using a perforated surface. The airflow after a shock wave flows to the wave-front through perforations, and the pressure before and after the shock wave can be automatically adjusted to reduce the intensity of the shock wave. This strategy, however, creates

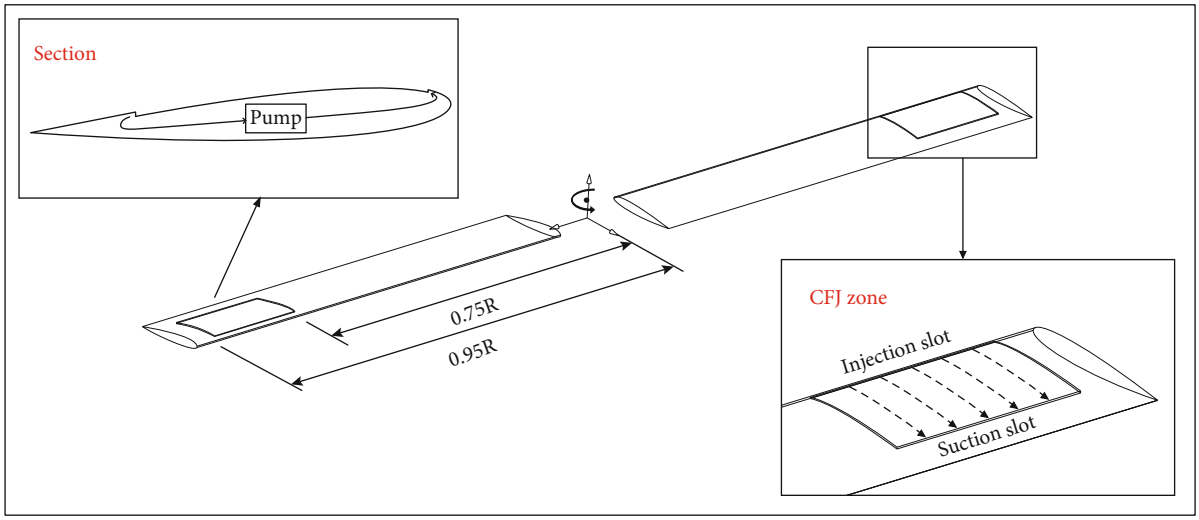

Figure 1: Helicopter rotor with CFJ control.

a boundary layer reflow, which dramatically increases viscous drag. In most circumstances, too much energy is lost, significantly compromising the reduction of wave resistance [9]. Passive control methods to suppress a flow separation of a retreating rotor at a high AoA are as follows: vortex generators [10, 11], gurney flaps [12, 13], wavy leading-edge [14, 15], and so on. Although these methods can suppress the flow separation of a rotor, this type of passive control works well in the design state, but when the working state deviates from the design point, the control effect is poor.

Active control methods act on a specific part of a rotor at a specific time. They can be actively adjusted, making the control more flexible. Thus, they have many advantages over passive control. The main active control methods for suppressing the flow separation of a rotor include active trailing-edge flaps [16, 17], inflatable leading edges [18, 19], variable-droop leading edges [20, 21], and synthetic jets [22–26]. However, active trailing-edge flaps and variable-droop leading edges often cause significant changes to the center of gravity and load. Moreover, they frequently necessitate intricate mechanical adjustment structures and control systems. A synthetic jet (acoustic wave or plasma) has a weak effect on the mainstream, and achieving continuous and efficient management is difficult. In general, suppressing the flow separation of a rotor has not been adequately addressed, and a more flexible and effective flow management system is urgently needed to improve the aerodynamic performance of rotors.

A coflow jet (CFJ) [27–29] is a new type of active flow control technology proposed by Zha of Miami University. In this method, the upper surface of the wing near the leading edge has a slot, which is used to inject a high-energy tangential jet in the same direction as the main flow. Then, flow with the same mass is drawn into another slot at the trailing edge. Pumps and pipes are arranged inside the wing to transport the air pulled in from the trailing edge to the injection slot at the leading edge. Since the rate at which air is blown out is equal to the suction rate, the CFJ is a zero-mass jet that does not require an additional air source. With the development of miniaturized motors and high-power technology, the proposed method has broad application. A CFJ has a lower cruise drag than a circulation control [30, 31] airfoil because it is not necessary to increase the circulation by blowing air onto the blunt leading or trailing edge (Coanda surface). In addition, a CFJ controls the flow around the airfoil more strongly than a synthetic jet, and the effect is more noticeable. In recent years, many scholars have studied CFJ control methods. Zha et al. found that CFJ can suppress the flow separation of a wing, improve the stall characteristics, and significantly increase the lift-to-drag ratio of the wing. Moreover, a CFJ has a high energy efficiency [28, 32]. Using particle image velocimetry, Wells [33] found that a CFJ can suppress the generation of airfoil wake vortices. Lefebvre [34, 35] designed a new electric aircraft concept based on CFJ control, which reduced the size of the wing, shortened the aircraft's take-off and landing distances, and increased the flight range. The latest research shows that a CFJ can also improve the aerodynamic performance of an airfoil in transonic conditions and increase its lift coefficient and lift-to-drag ratio [36, 37].

When a rotor rotates through a circle, a flow separation can occur for a retreating blade at a high AoA whereas a flow separation of the advancing blade can be induced by a shock wave. Research shows that a CFJ effectively suppresses the flow separation of a fixed wing at high AoAs and reduces the transonic separation. Therefore, using CFJ may be a promising flow control strategy for suppressing both the shock-induced flow separation of the advancing blade and the flow separation of the retreating blade at large AoAs. Yang et al. [38], Xu et al. [39], Liu et al. [40, 41], etc. found that CFJ control weakened the flow separation and improved the aerodynamic performance of a rotor airfoil.

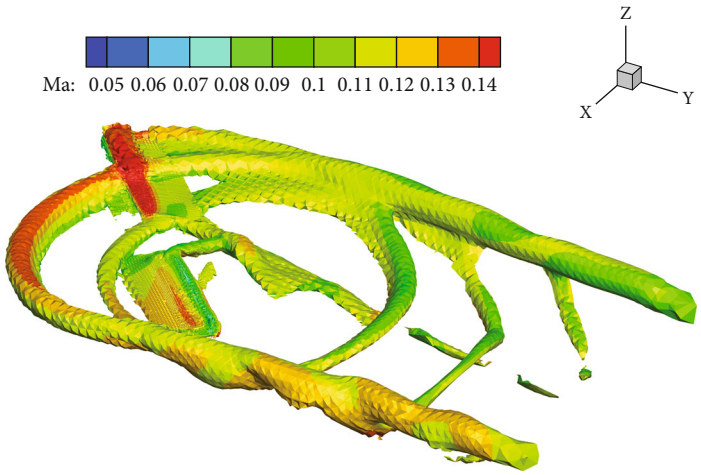

Figure 2: Vorticity isosurface contour of the AH-1/OLS rotor (colored by Mach number).

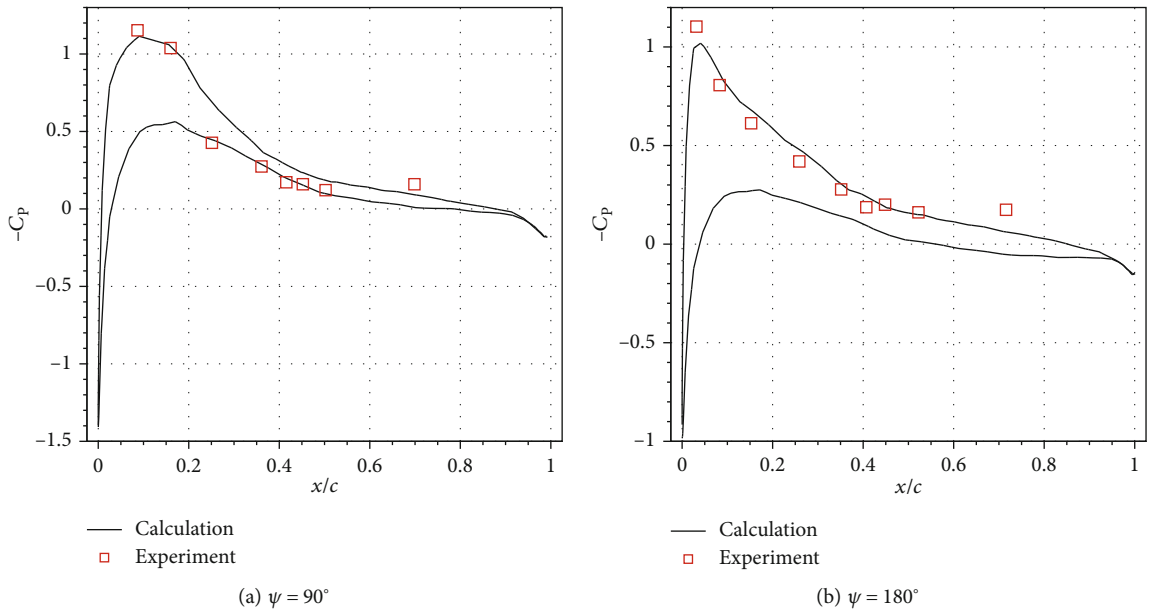

Figure 3: Surface pressure coefficient vs. dimensionless position for the AH-1/OLS rotor at $r = 0.955R$.

However, current research has considered only two-dimensional airfoils, and there has been very little research published on the flow separation control of a three-dimensional rotor. Therefore, more research into the control effect and mechanism of this method are required.

In this work, flow separation suppression and aerodynamic performance improvement for a three-dimensional helicopter rotor based on a CFJ positioned at the rotor tip is investigated using the numerical simulation method. The mechanism of action is also explored. Further, the effects of the jet momentum coefficient of the CFJ and the location, width, and height of the slots are investigated. The rest of this paper is organized as follows. The CFJ control method for the rotor and the numerical simulation of a rotor flow field with CFJ control are introduced in Section 2. The results for flow separation suppression and aerodynamic performance improvement of a rotor with CFJ control are described in Section 3 for rotors in typical states. The effects of different values of the CFJ control parameters on aerodynamic performance improvement for a rotor are studied in Section 4. The entire work is summarized in Section 5.

2. Methodology

2.1. Rotor Model with CFJ Control. A rotor with CFJ control is shown schematically in Figure 1. The leading edge of the rotor has a slot through which air is blown out. The trailing edge has a slot into which air is sucked. The surface of the rotor between the injection slot and the suction slot was created by translating and rotating the surface of the original rotor. In addition, note that for CFJ control, the jet

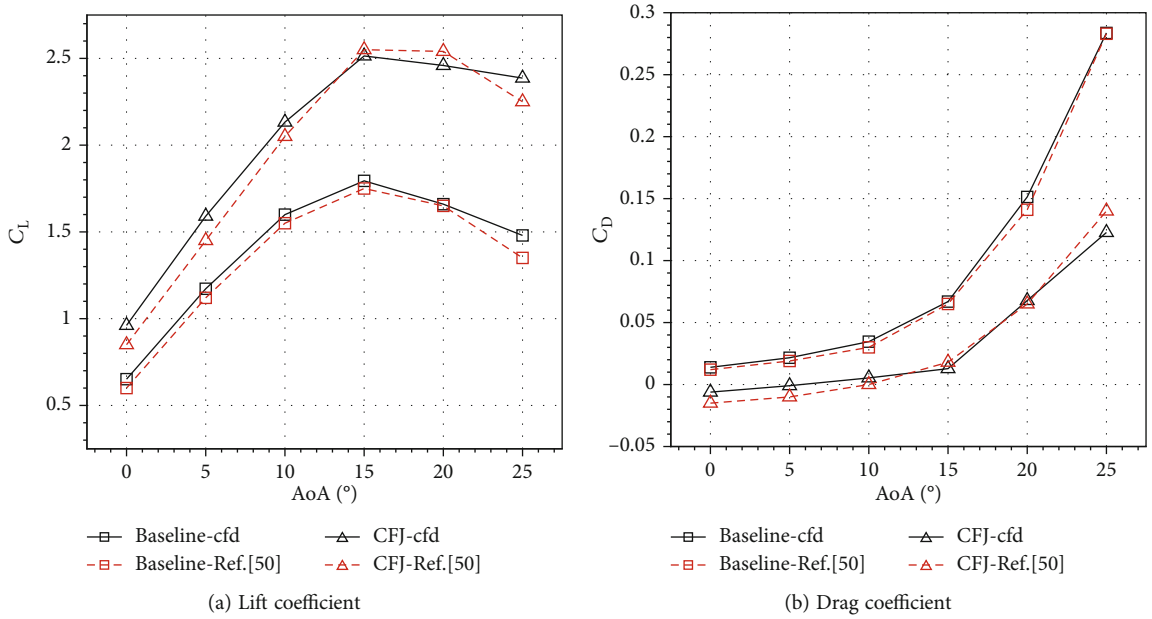

(a) Lift coefficient (b) Drag coefficient

Figure 4: Lift and drag coefficients vs. AoA for a NACA6415 airfoil with and without CFJ control.

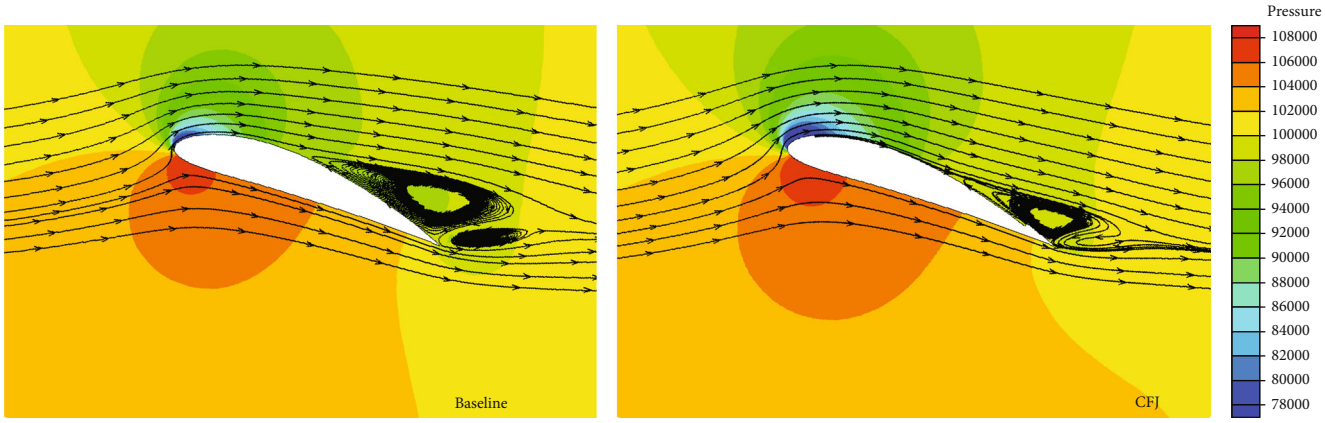

Figure 5: Pressure contours and streamlines of a NACA6415 airfoil without (a) and with CFJ control (b) for AoA = 20°.

momentum coefficient is commonly employed to describe the intensity of the airflow. It is defined as:

$$C_\mu = \frac{\dot{m}V_j}{1/2\rho_\infty V_\infty^2 S}, \tag{1}$$

where $\dot{m}$ is the mass flow rate, V_j is the jet velocity at the injection slot, ρ_∞ is the density of the free stream, V_∞ is the velocity of the free stream, and S is the reference area of the rotor.

2.2. Numerical Methods. The flow field around a helicopter rotor was simulated using the compressible Reynolds-averaged Navier–Stokes equations, whose integral form can be written as

$$\frac{\partial}{\partial t}\int_\Omega \mathbf{W}d\Omega + \oint_{\partial\Omega}(\mathbf{F_C} - \mathbf{F_V})dS = 0, \tag{2}$$

where Ω is the control volume, $\partial\Omega$ is the boundary of the control volume, $\mathbf{W}$ are the conservative variables, and $\mathbf{F_C}$ and $\mathbf{F_V}$ are the convective fluxes and viscous fluxes:

$$W = \begin{pmatrix} \rho \\ \rho u \\ \rho v \\ \rho w \\ \rho E \end{pmatrix}, F_C = \begin{pmatrix} \rho V_r \\ \rho u V_r + n_x p \\ \rho v V_r + n_y p \\ \rho w V_r + n_z p \\ \rho H V_r + V_t p \end{pmatrix}, F_V = \begin{pmatrix} 0 \\ n_x\tau_{xx} + n_y\tau_{xy} + n_z\tau_{xz} \\ n_x\tau_{yx} + n_y\tau_{yy} + n_z\tau_{yz} \\ n_x\tau_{zx} + n_y\tau_{zy} + n_z\tau_{zz} \\ n_x\Theta_x + n_y\Theta_y + n_z\Theta_z \end{pmatrix}, \tag{3}$$

where u, v, and w are the three components of the velocity in the x, y, and z directions. ρ, p, E, and H are the density, pressure, the total energy per unit mass, and the total enthalpy per unit mass, respectively. n_x, n_y, and n_z are the components of the unit normal vector of

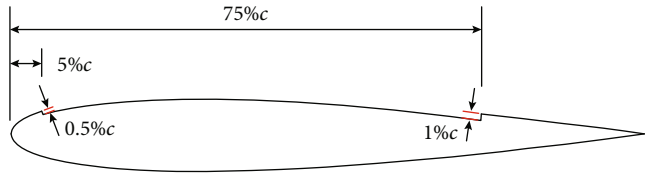

Figure 6: Profile of a CFJ-based rotor showing the positions and heights of the two slots.

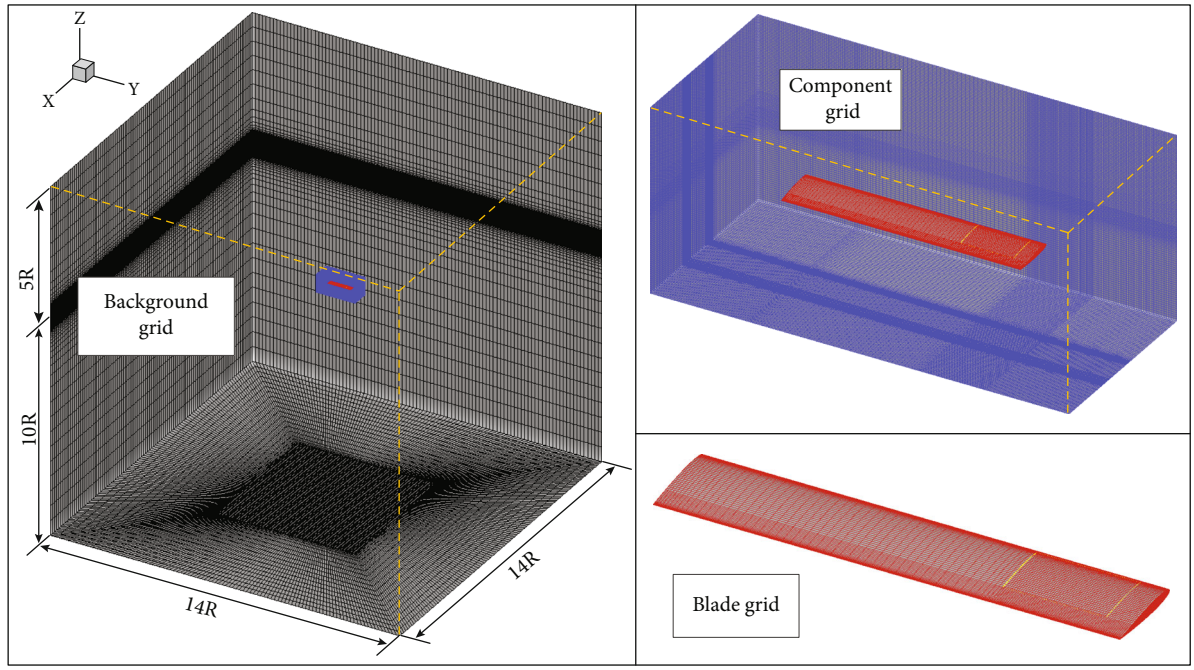

(a) Overset grid

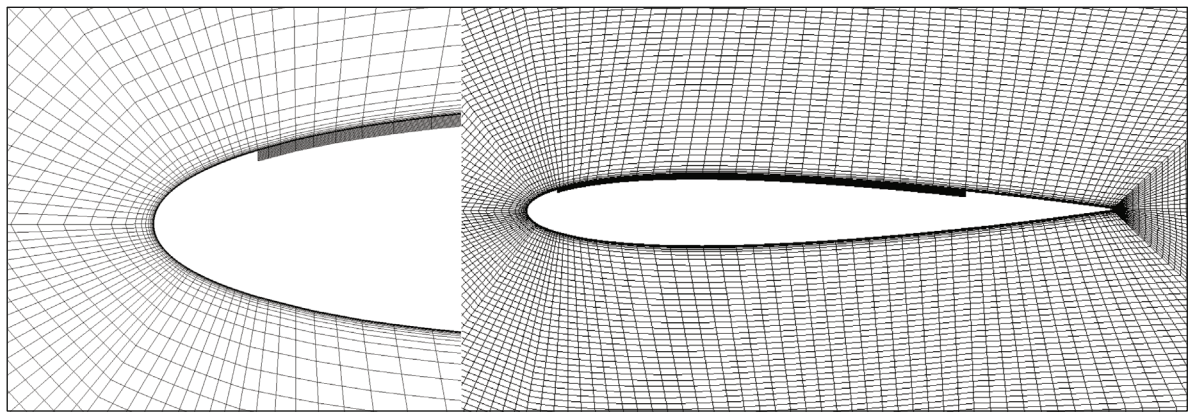

(b) Grid around the airfoil at CFJ slice

Figure 7: Computational domain and overset grid.

the control volume surface. V_r is the relative velocity, and V_t is the grid velocity. τ_{ij} is the component of the viscous stress tensor. Θ_i is a term that describes the work of the viscous stress and the heat conduction in the fluid. Further details of the equations can be found in Ref. [42].

In this work, the finite volume method was employed to solve the governing equations of the fluid. The Roe scheme [43] was adopted to discretize the convective fluxes. The discrete fluxes at each face are given by:

$$\mathbf{F}_{1/2} = \frac{1}{2}(\mathbf{F}(\mathbf{W}_\mathbf{R}) + \mathbf{F}(\mathbf{W}_\mathbf{L})) - \frac{1}{2}|\mathbf{A}|(\mathbf{W}_\mathbf{R} - \mathbf{W}_\mathbf{L}), \quad (4)$$

where $\mathbf{F}_{1/2}$ are the inviscid fluxes over the face of the control volume, $\mathbf{W}_\mathrm{L}$ and $\mathbf{W}_\mathbf{R}$ denote the left and right states, and $\mathbf{A}$

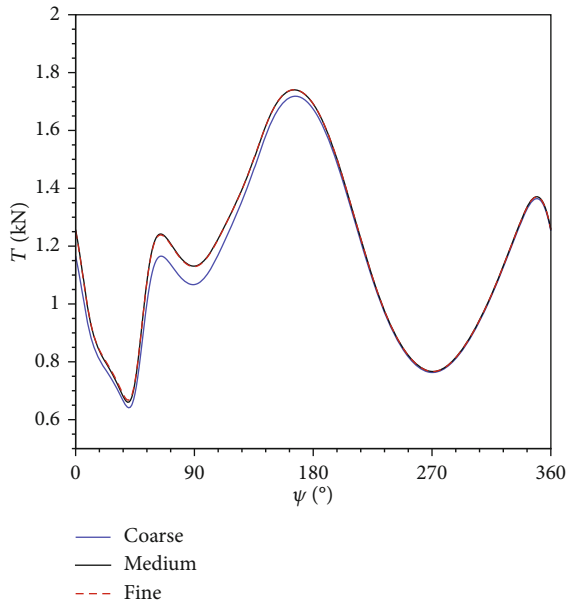

Figure 8: Thrust of a C-T rotor vs. azimuth angle computed for the three grid resolutions.

denotes the Roe matrix. The viscous fluxes were discretized by a second-order central difference.

To simulate the unsteady flow simulation of rotor, the dual time-stepping method [44] was used for time discretization. The time derivative term of Equation (2) is approximated by the 3-point backward difference scheme to obtain the implicit equation; the formula is as follows:

$$\frac{3\mathbf{W}^{n+1} - 4\mathbf{W}^{n} + \mathbf{W}^{n-1}}{2\Delta t} + \mathbf{R}\left(\mathbf{W}^{n+1}\right) = 0, \tag{5}$$

where Δt represents the global physical time step, which was set as the time corresponding to a rotation of the rotor by 1°. In order to solve the nonlinear implicit equation, a pseudo-time derivative term was introduced, and then, the time marching method used in the steady equation was used to solve it. The following formula can be obtained.

$$\begin{aligned} &\frac{d\left(\Omega^{n+1}\mathbf{W}^{*}\right)}{d\tau} + \mathbf{R}^{*}\left(\mathbf{W}^{*}\right) = 0, \\ &\mathbf{R}^{*}\left(\mathbf{W}^{*}\right) = \mathbf{R}\left(\mathbf{W}^{*}\right) + \frac{3\mathbf{W}^{*} - 4\mathbf{W}^{n} + \mathbf{W}^{n-1}}{2\Delta t}, \end{aligned} \tag{6}$$

where $\mathbf{R}$ and $\mathbf{R}^{*}$ represent the residual, τdenotes a pseudo-time variable.

The two-equation turbulence model with $k-\omega$ SST [45] was employed to simulate the separated airflow over the surface of the helicopter rotor. A no-slip boundary condition was applied for the rotor surface, and a nonreflection boundary condition was applied for the far field.

An overset grid [46, 47] was used to simulate the motion of the rotor, as this technique works well for complex moving-body problems [48]. An overset grid consists of a background grid and a component grid. Each set of grid is generated separately, which not only makes grid generation easier but also ensures that grid quality is maintained throughout grid movement. The computational grid was established at each time step by performing three steps: hole mapping, searching for contributing cells, and interpolation.

2.3. Validation of the Numerical Methods. In this section, the flow field of an AH-1/OLS rotor in forward flight and a NACA6415 airfoil with CFJ control were computed to ensure that the methodology is correct, laying the groundwork for the numerical simulation of the rotor's flow field based on CFJ control.

2.3.1. AH-1/OLS Rotor in Forward Flight. The AH-1/OLS rotor is composed of two blades with an Operational Loads Survey (OLS) airfoil. The rotor radius $R = 0.958$ m and chord $c = 0.104$ m. The linear negative torsion of the blade is 10°, and the blade root is removed by 18.2%. Experimental case 10014 in Ref. [49] is selected for calculation: the Mach number of the rotor tip $\mathrm{Ma}_{\mathrm{tip}} = 0.664$, Reynolds number $\mathrm{Re} = 1.6 \times 10^{6}$, advance ratio $\mu = 0.164$, and tip-path plane angle is 1°. The trimmed periodic pitching and flapping angles are as follows:

$$\begin{aligned} \theta(t) &= 6.14^{\circ} + 0.9^{\circ}\cos\psi(t) - 1.39^{\circ}\sin\psi(t), \\ \beta(t) &= 0.5^{\circ} - 1^{\circ}\cos\psi(t). \end{aligned} \tag{7}$$

The numbers of background and component grid elements were 1.8×10^{6} and 6.1×10^{6}, respectively. Figure 2 shows the vorticity isosurface contour of the AH-1/OLS rotor (colored by Mach number). It can be seen that the numerical method use for the rotor flow field in this paper simulates the tip vortex of the rotor well. Figure 3 gives the surface pressure coefficient distribution of the $0.955R$ section at azimuth angles of 90° and 180°. In the figure, C_p is the

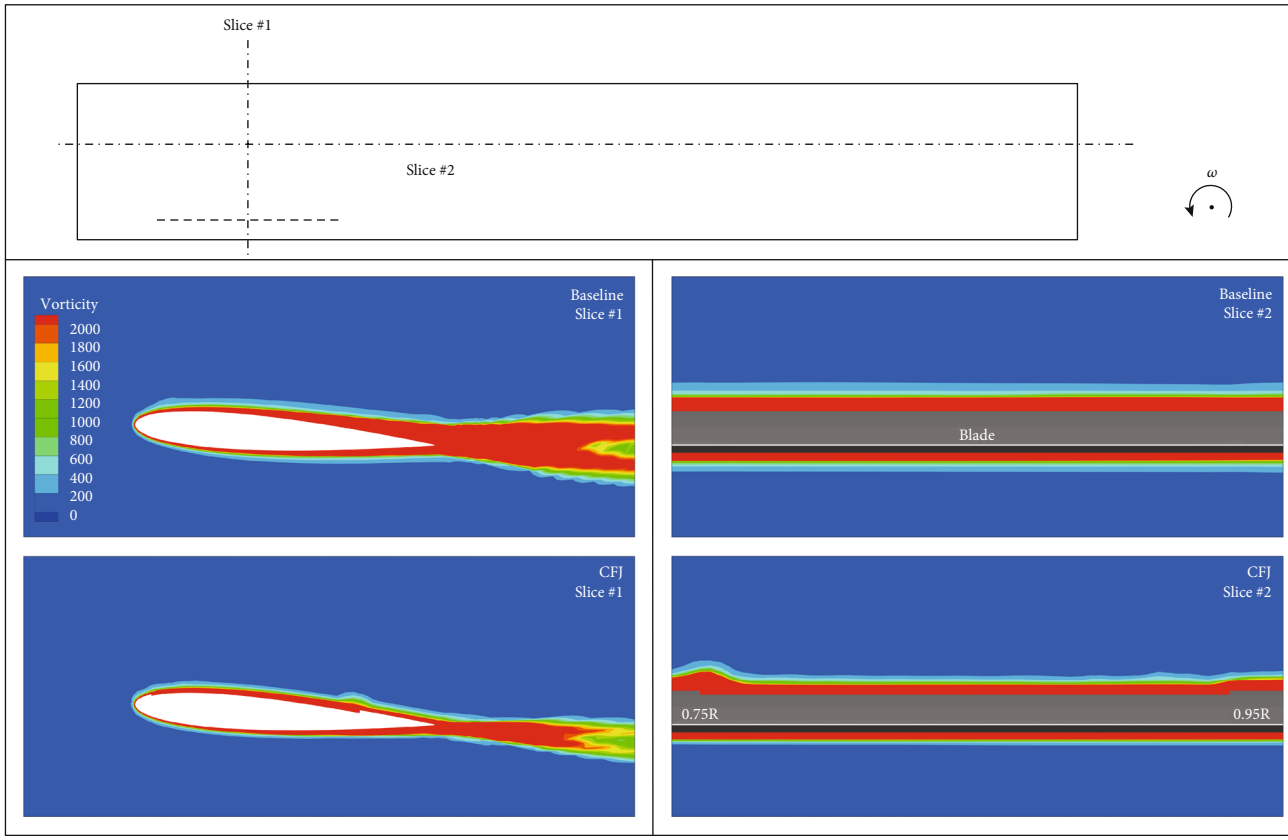

(a) $\Psi = 90^{\circ}$

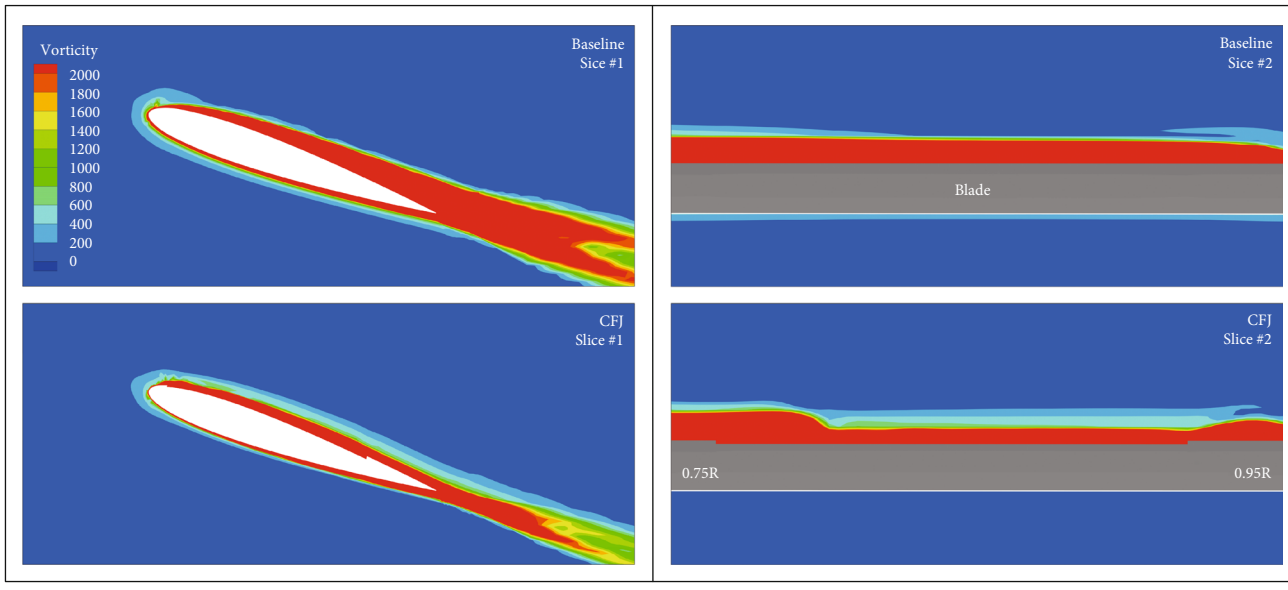

(b) $\Psi = 270^{\circ}$

Figure 9: Vorticity contours of the rotor slices.

pressure coefficient, and x/c is the dimensionless position along the chord line. The calculated results are in good agreement with the experimental data as shown in the figure, which verifies the correctness of the numerical simulation of the rotor flow field.

2.3.2. Coflow Jet Flow Control. The NACA6415 airfoil with CFJ control [50] was selected to be another validation case. In the computation, Mach number Ma = 0.3, Reynolds number $\mathrm{Re} = 2.08 \times 10^6$, and jet momentum coefficient $C_\mu = 0.08$. The lift coefficient (C_L) and drag coefficient (C_D)

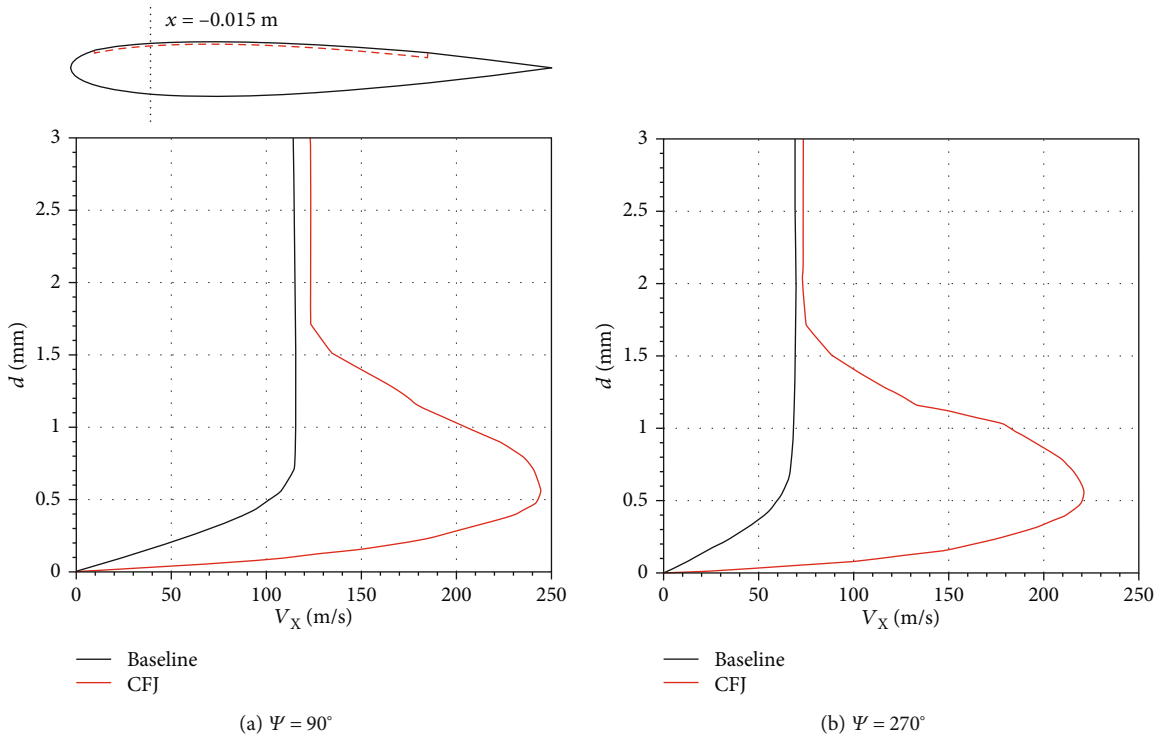

Figure 10: Velocity profiles of the baseline and CFJ-based rotor slices for $r = 0.85R$ and $x = -0.015$ m.

of a NACA6415 airfoil obtained for AoA = 0°, 5°, 10°, 15°, 20°, and 25° are shown in Figure 4. It can be seen that the computational fluid dynamics (CFD) results from our simulation at different AoAs fit the results of Ref. [50] well, which means the present simulation method is correct. Figure 5 presents the pressure contours and the streamlines of a NACA6415 airfoil with or without CFJ at AoA = 20°. It is apparent that the flow separation at the trailing edge of the airfoil was well suppressed by the CFJ.

3. CFJ Control of Helicopter Rotor under Typical Flight Conditions

In this work, a helicopter rotor with CFJ control was based on a Caradonna–Tung (C-T) rotor [51] as the original model. The flow separation and aerodynamic performance improvement of the rotor with CFJ control were investigated. Only one rotor blade was simulated to demonstrate the effect of CFJ control better. A model of the C-T rotor with CFJ control is shown in Figure 1. The width of the CFJ slot was $0.2R$, and the slot was positioned between $0.75R$ and $0.95R$. The profile of the CFJ-based rotor is shown in Figure 6. The Mach number of the rotor tip $Ma_{tip} = 0.6$ and the advance ratio $\mu = 0.3$. The trimmed periodic pitching angle was $\alpha(t) = 12° - 8° \sin(\omega t)$. The jet momentum coefficient $C_\mu = 0.0138$. Figure 7 shows the computational domain and the overset grid.

3.1. Verification of Grid Independence. First, in this section, grid independence was investigated. The number of background grid elements was 1.7×10^6. Three grids were employed, a coarse grid, a medium grid, and a fine grid. The numbers of grid elements were 3.0×10^6, 4.1×10^6, and 5.3×10^6, respectively. Figure 8 shows that the thrust of a C-T rotor computed with the three grid resolutions was in phase. As can be seen, there was a significant deviation of the thrust calculated with the coarse grid compared to the other two grids at 90°. The results for the medium grid are almost the same as those for the fine grid. Therefore, the medium grid has sufficient resolution and was used in following simulations.

3.2. Flow Field Analysis of Helicopter Rotor. Figure 9 presents the vorticity contours of rotor slices at azimuths of 90° and 270°. Slice 1 is in the middle of the CFJ zone ($r = 0.85R$) and slice 2 is $0.58c$ away from the leading edge of the blade. The vorticity around the rotor decreased after applying CFJ control at an azimuth of 90° or 270°. The separation vortex on the upper surface was obviously suppressed at 270° where the rotor has a high AoA. Besides, slice 2 shows that the zone where the separation vortex weakened moved to the tip of the blade relative to the CFJ zone ($0.75R$–$0.95R$), which was caused by the large centrifugal force generated by the high-speed rotation of the rotor.

Figure 10 shows the velocity profiles of the upper surfaces of the baseline and CFJ-based rotors ($r = 0.85R$) behind the injection slot at $x = -0.015$ m. Here, d is the distance from the upper surface of the rotor, and V_X is the velocity along the chord direction of the rotor. The panels indicate that the main flow velocity on the leading edge increased when the airflow was blown from the injection slot and that the velocity profile in the near-wall region was fuller, which enhanced the ability of the blade to resist the adverse

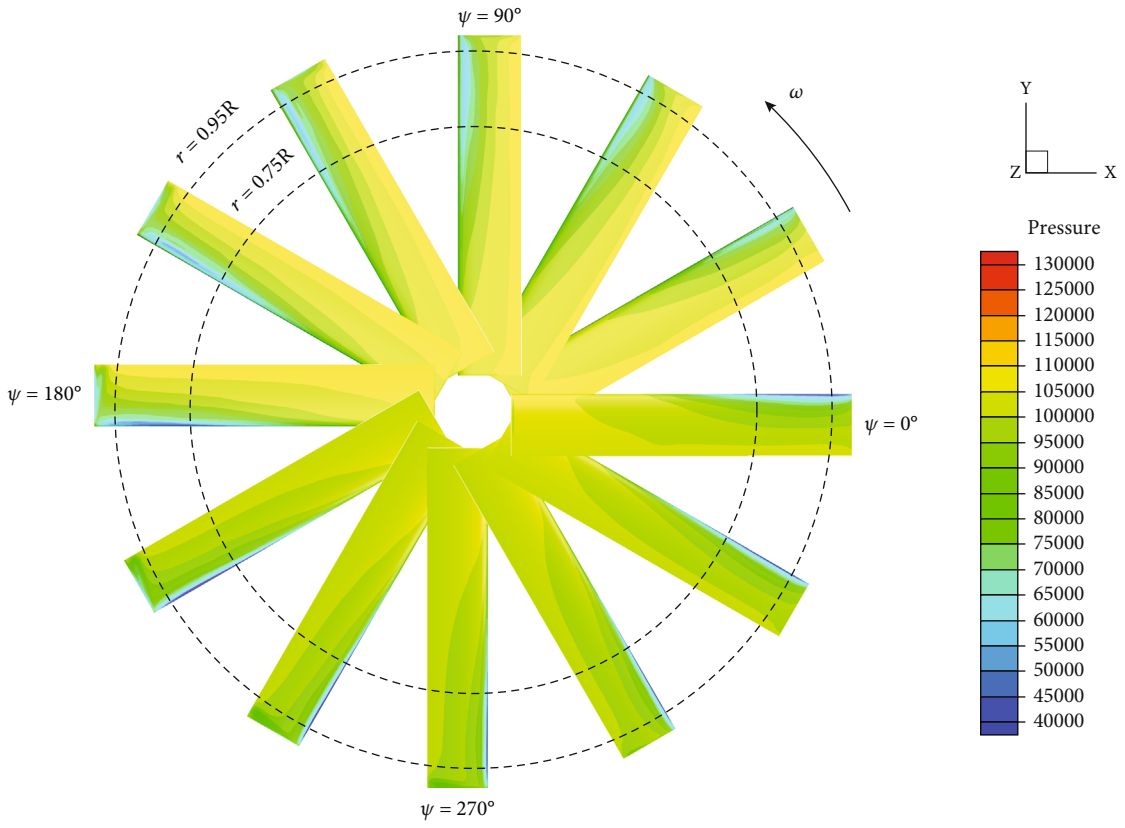

(a) Baseline rotor

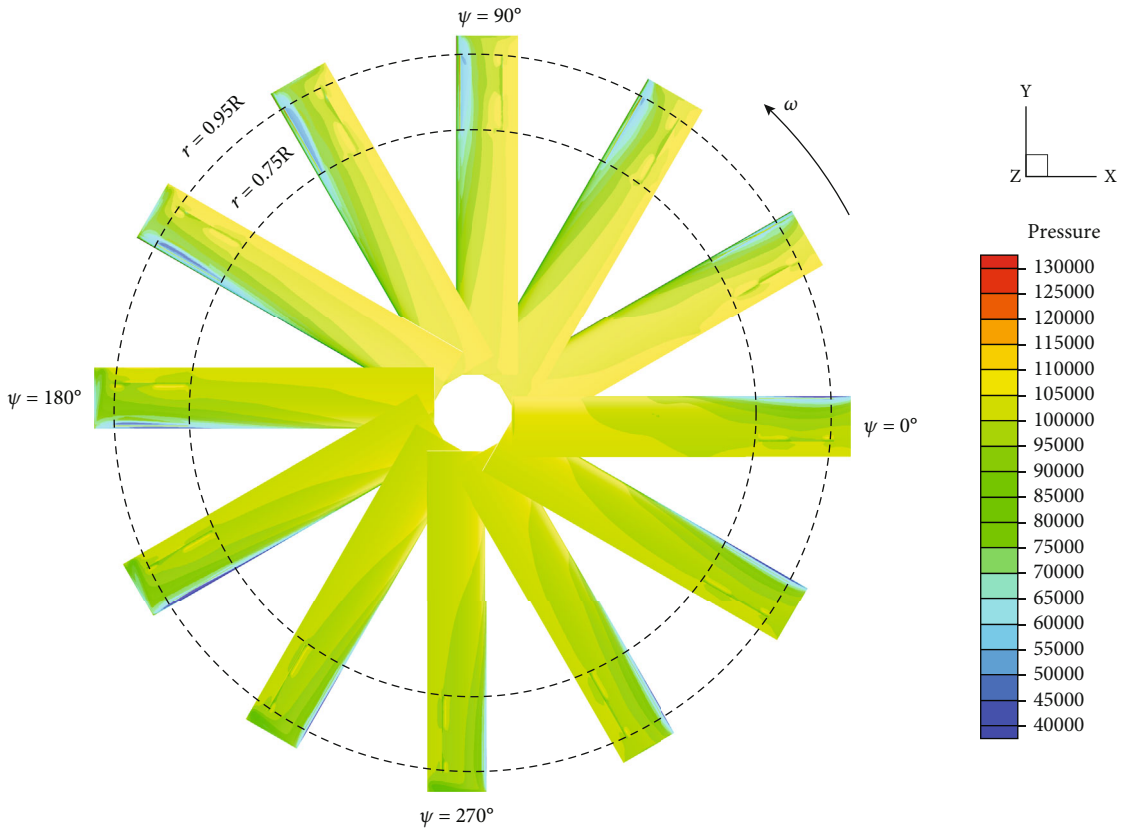

(b) CFJ-based rotor

Figure 11: Pressure contours of the baseline rotor and the CFJ-based rotor.

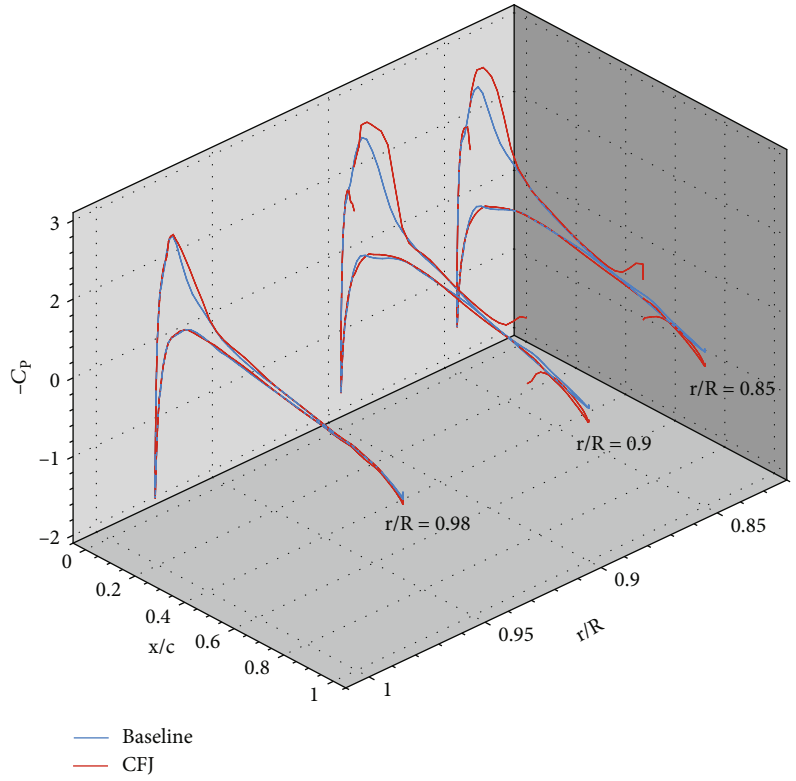

(a) $\Psi = 90^\circ$

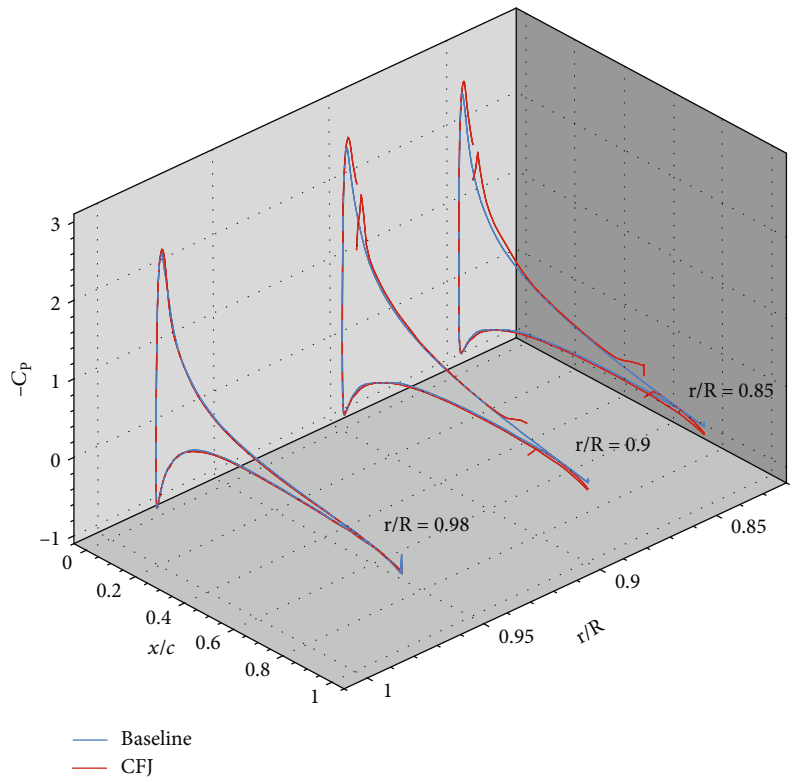

(b) $\Psi = 270^\circ$

Figure 12: Surface pressure coefficient of the baseline rotor and CFJ-based rotor.

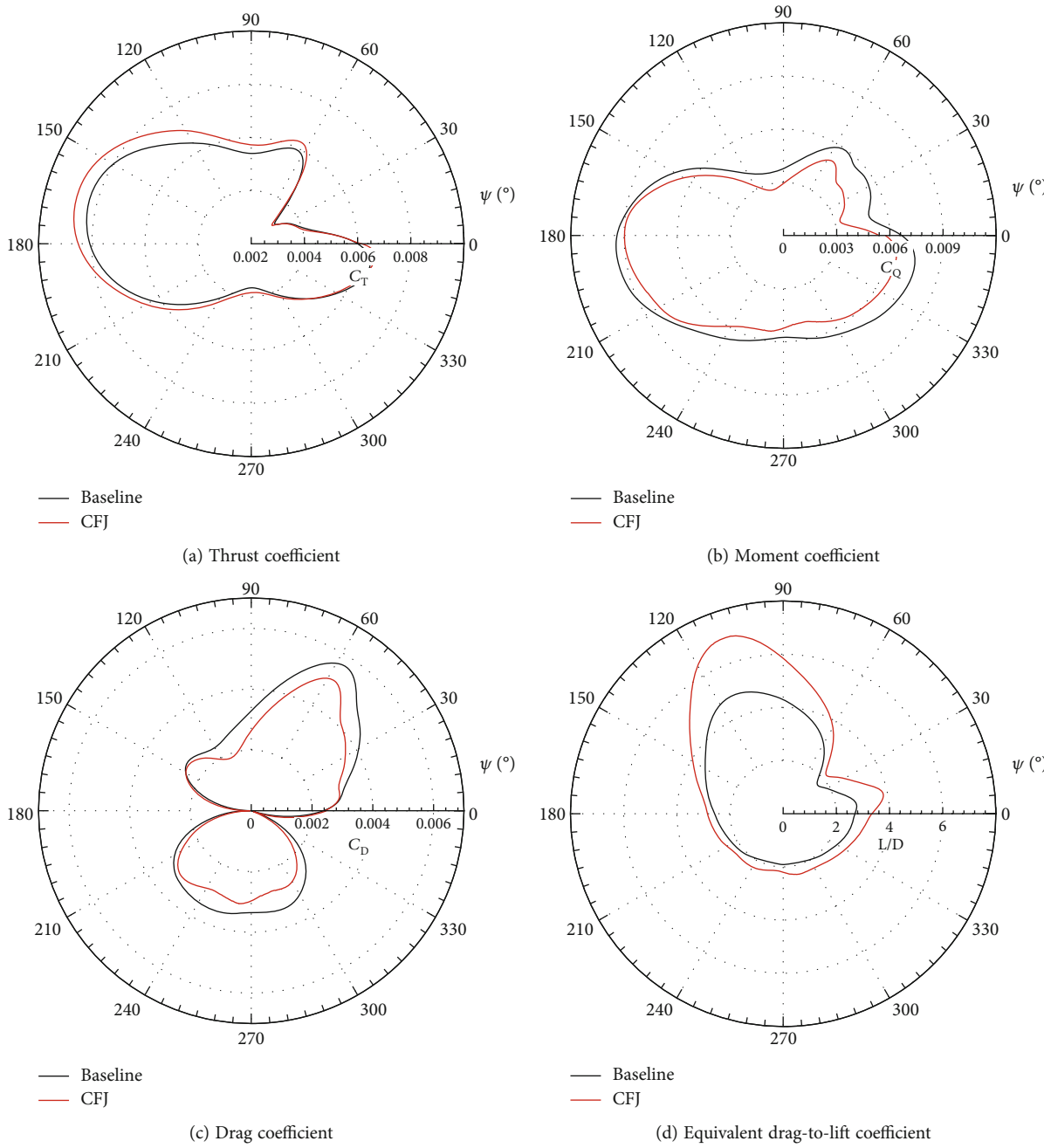

(a) Thrust coefficient

(b) Moment coefficient

(c) Drag coefficient

(d) Equivalent drag-to-lift coefficient

Figure 13: Aerodynamic coefficients of the baseline rotor and CFJ-based rotor.

pressure gradient and effectively suppressed the flow separation on the upper surface of the rotor.

Figure 11 shows the pressure contours of the rotor surface with and without CFJ control. It is apparent that the surface pressure between the injection slot and the suction slot of the CFJ-based rotor was lower than in the corresponding part of the baseline rotor. The closer to the tip of the blade, the more the lower pressure zone increased along the chord length. In addition, the surface pressure of the area outside the CFJ zone ($0.1R$–$0.75R$ and $0.95R - R$) also decreased.

Figure 12 presents the surface pressure coefficient of the baseline rotor and CFJ-based rotor at an azimuth of 90° or 270°. The distribution of the surface pressure for the profiles at $0.85R$ and $0.9R$ is significantly different between the baseline rotor and CFJ-based rotor at the azimuth of 90°. The surface pressure coefficient between the injection slot and $0.3c$ and between $0.6c$ and the suction slot dropped strikingly with CFJ control. Furthermore, the surface pressure coefficient at $0.98R$, which is outside the CFJ zone, was slightly lower. At the azimuth angle of 270°, the surface pressure of the CFJ-based rotor decreased less than that of the baseline rotor at 90°. The surface pressure coefficient between $0.1c$ and $0.3c$ and between $0.6c$ and the suction slot decreased with CFJ control for the profiles at $0.85R$ and $0.9R$. The difference in the surface pressure coefficient

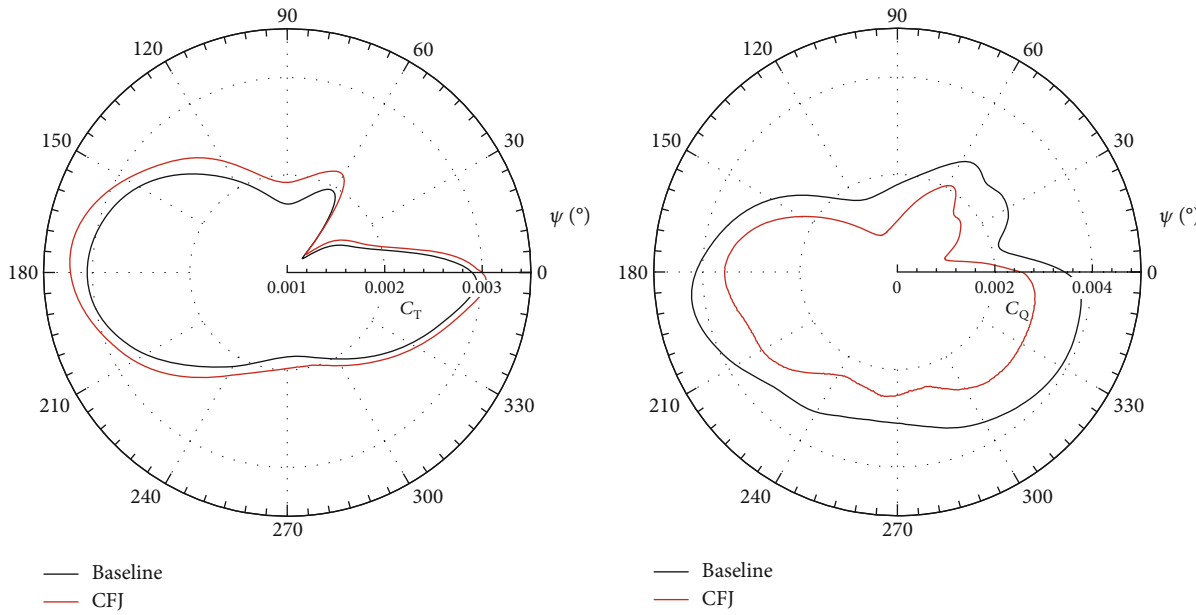

(a) Thrust coefficient

(b) Moment coefficient

Figure 14: Thrust and moment coefficients in the CFJ zone (0.75R–0.95R).

between the baseline rotor and the CFJ-based rotor was small for the profile at 0.98R.

3.3. Aerodynamic Performance Improvement of Helicopter Rotor. The effect of CFJ control on improving the aerodynamic performance of a rotor was mainly analyzed by assessing the change in the unsteady aerodynamic coefficients. The main aerodynamic coefficients of a rotor are the thrust coefficient C_T, moment coefficient C_Q, drag coefficient C_D, and equivalent lift-to-drag ratio $(L/D)_e$:

$$C_T = \frac{T}{\rho\pi R^2(\omega R)^2}, \tag{8}$$

$$C_Q = \frac{Q}{\rho\pi R^3(\omega R)^2}, \tag{9}$$

$$C_D = \frac{D}{\rho\pi R^2(\omega R)^2}, \tag{10}$$

$$\left(\frac{L}{D}\right)_e = \frac{C_T}{C_Q/\mu}, \tag{11}$$

where T, Q, and D are the thrust, moment, and drag of the rotor, respectively. ρ is the density of free flow, μ is the advance ratio, and ω is the angular velocity.

For the CFJ rotor, power consumption should be considered. And Equation (10) changes as the following:

$$C_D = \frac{D + P/V_{\text{tip}}}{\rho\pi R^2(\omega R)^2}, \tag{12}$$

where P is the power required by the pump. V_{tip} is the velocity of the rotor tip. And P is defined as:

$$P = \frac{\dot{m}c_p T_0}{\eta}\left(\left(\frac{P_{\text{in}}}{P_{\text{suc}}}\right)^{(\gamma-1)/\gamma} - 1\right), \tag{13}$$

where $\dot{m}$ is the jet mass flow rate. c_p is the constant pressure specific heat. T_0 is the total temperature. η is the efficiency of the pump and equals to 0.9 in this work. P_{in} and P_{suc} are the total pressure of injection and suction slots. γ is the air specific-heats ratio.

The aerodynamic coefficients of the baseline rotor and CFJ-based rotor are shown in Figure 13. The thrust coefficient of the rotor had increased for all azimuth angles after applying CFJ control. On the advancing side, the greatest increase of about 5.6% was near the azimuth angle of 90°. On the retreating side, the greatest increase of about 4.8% was near the azimuth angle of 270°. The moment coefficient decreased over the whole period. On the advancing side, the greatest decrease of about 26.8% was at the azimuth angle of 100°. On the retreating side, the greatest decrease of about 16.0% was at the azimuth angle of 280°. The drag coefficient was also significantly reduced over the whole period. On the advancing side, the greatest decrease of about 27.3% was at 100°. On the retreating side, the greatest decrease of about 20.8% was at 280°. As the thrust coefficient of the rotor increased and the moment coefficient decreased after using CFJ control, the equivalent lift-to-drag ratio of the rotor increased significantly, by about 44.0% at 90° on the advancing side and by 15.3% at 270° on the retreating side. In general, CFJ control significantly improved the aerodynamic performance of the rotor.

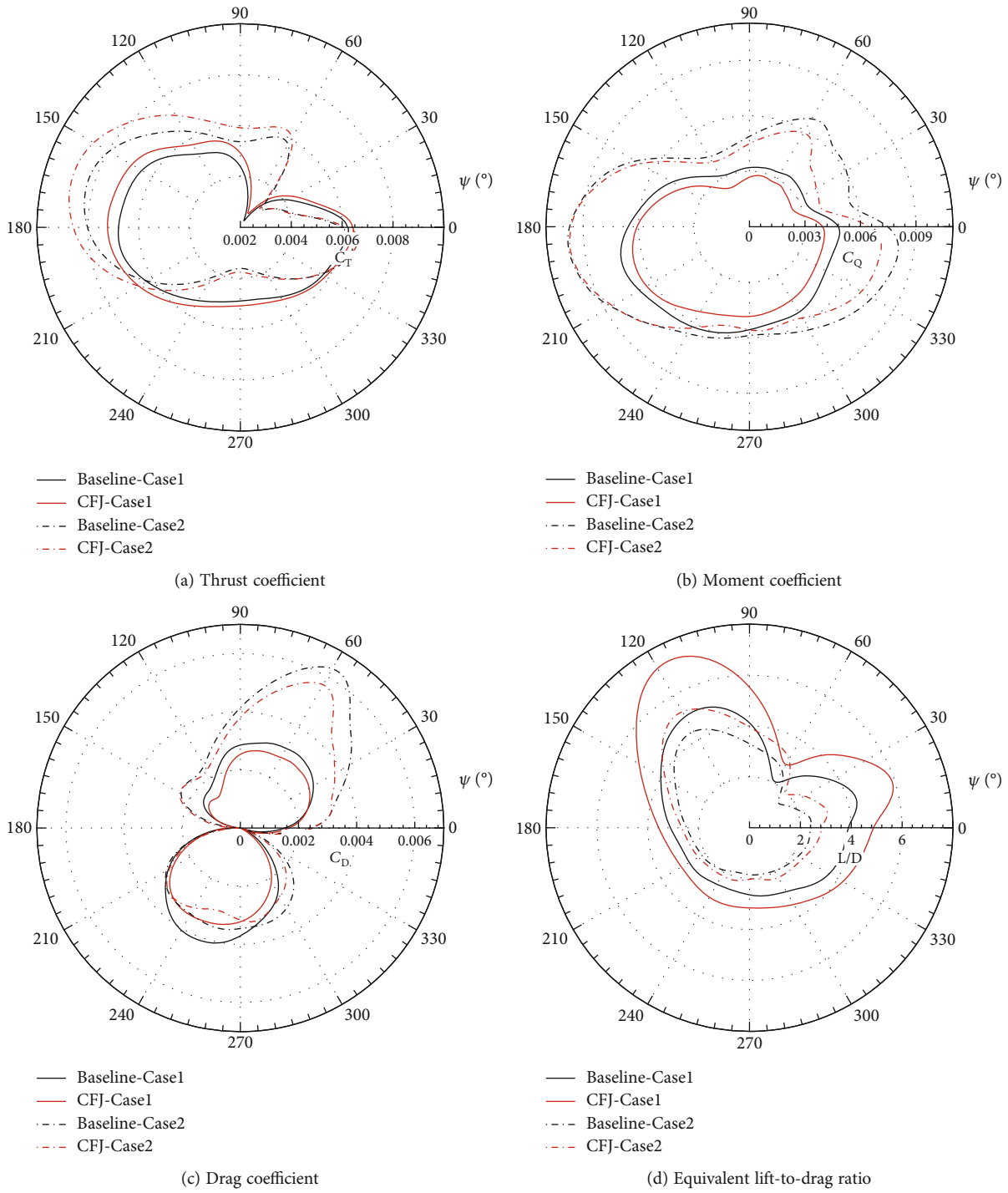

Figure 15: Aerodynamic coefficients of the baseline rotor and CFJ-based rotor under different flight conditions.

To make the changes in the aerodynamic coefficients more apparent visually, Figure 14 shows the thrust and moment coefficients in the CFJ zone ($0.75R$–$0.95R$). The thrust coefficient in the CFJ zone has noticeably increased. The maximum increases were about 13.0% near the azimuth of 90° on the advancing side and 6.2% near the azimuth of 270° on the retreating side. Furthermore, the moment coefficient decreased substantially. The maximum decreases were about 49.2% at the azimuth of 100° on the advancing side and 26.3% at the azimuth of 280° on the retreating side.

To verify that CFJ control can generally improve the aerodynamic performance of a rotor under different flight conditions, cases with a different advance ratio or a different Mach number were investigated (case 1: $Ma_{tip} = 0.6$, $\mu = 0.2$; case 2: $Ma_{tip} = 0.65$, $\mu = 0.3$).

The aerodynamic parameters of the baseline rotor and CFJ-based rotor are compared in Figure 15. Aerodynamic

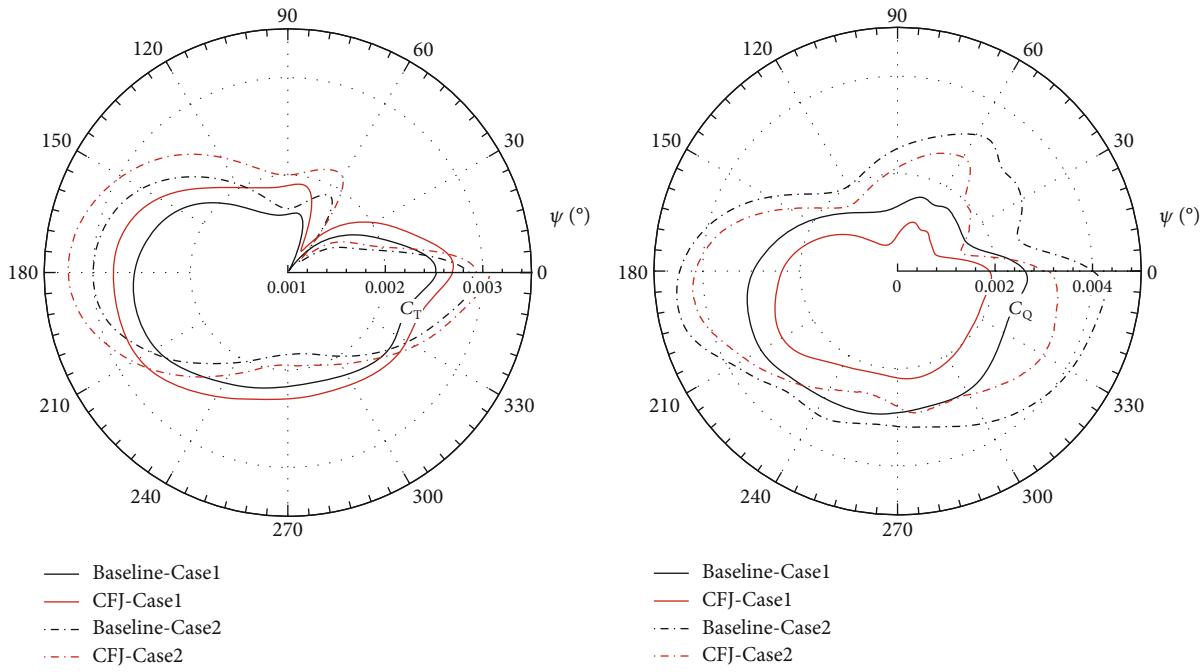

(a) Thrust coefficient

(b) Moment coefficient

Figure 16: Thrust and moment coefficients in the CFJ zone (0.75R–0.95R).

performance of the rotor under different flight conditions was improved with CFJ control, that is, the thrust coefficient increased, the moment coefficient decreased, the drag coefficient decreased, and the equivalent lift-to-drag ratio increased. However, the increment of the thrust coefficient between the azimuth angles of 300° and 30° was less compared to other azimuth angles. The decrement of the moment coefficient in case 2 between azimuths of 120° and 240° was less than that of case 1. Thus, the increment of the equivalent lift-to-drag ratio was reduced within this range of azimuth angles.

Next, the change in the aerodynamic coefficients of a rotor in the CFJ zone (0.75R–0.95R) was investigated, specifically to analyse the control effect of CFJ. Figure 16 compares the thrust and moment coefficients of the baseline rotor and CFJ-based rotor in the CFJ zone. In case 1, the thrust coefficient of the rotor with CFJ control had significantly increased over the whole period, and the moment coefficient had significantly decreased. However, the increment of the rotor thrust coefficient was small for azimuth angles of 0°–30° for case 2, which has a higher Mach number at the rotor tip and a larger advance ratio than case 1. Further, the decrement of the rotor moment coefficient was small for the azimuth angles 180°–240°.

4. Effects of CFJ Parameters on Aerodynamic Performance of Helicopter Rotor

To further explore the effect of the CFJ parameters on the aerodynamic performance improvement of the rotor, CFJ cases with different jet momentum coefficients, locations, widths, and heights of the injection and suction slots are explored in this section.

4.1. Effect of CFJ Momentum Coefficient. The effect of the CFJ momentum coefficient on the aerodynamic performance of the rotor is investigated in this section. The position, width, and height of the CFJ injection and suction slots are the same as those in Section 3. The jet coefficient was 0.0097, 0.0138, or 0.0196. Figure 17 shows the thrust and moment coefficients of the baseline rotor and CFJ-based rotor with different jet momentum coefficients. The results show that, for most azimuth angles, the thrust coefficients of the CFJ-based rotors were larger than that of the baseline rotor whereas the moment coefficients of the CFJ-based rotors were smaller than that of the baseline rotor. These coefficients were almost equal for the different rotors at other azimuth angles. The greater the jet momentum coefficient, the greater the increase in the rotor thrust coefficient, and the greater the decrease in the rotor moment coefficient compared to the baseline rotor. The increase of the thrust coefficient of the rotor near the azimuth angle of 90° on the advancing side was more pronounced than near 270° on the retreating side. The reduction of the moment coefficient of the rotor near the azimuth angle of 270° on the retreating side was more pronounced than on the advancing side near 90°.

4.2. Effect of CFJ Location. The effect of the location of the CFJ on the aerodynamic performance of the rotor is investigated in this section. The symmetry plane of the CFJ was at $r = 0.79R$, $0.85R$, or $0.88R$, and the slot width was $0.2R$. According to the distance of the CFJ from the rotor tip,

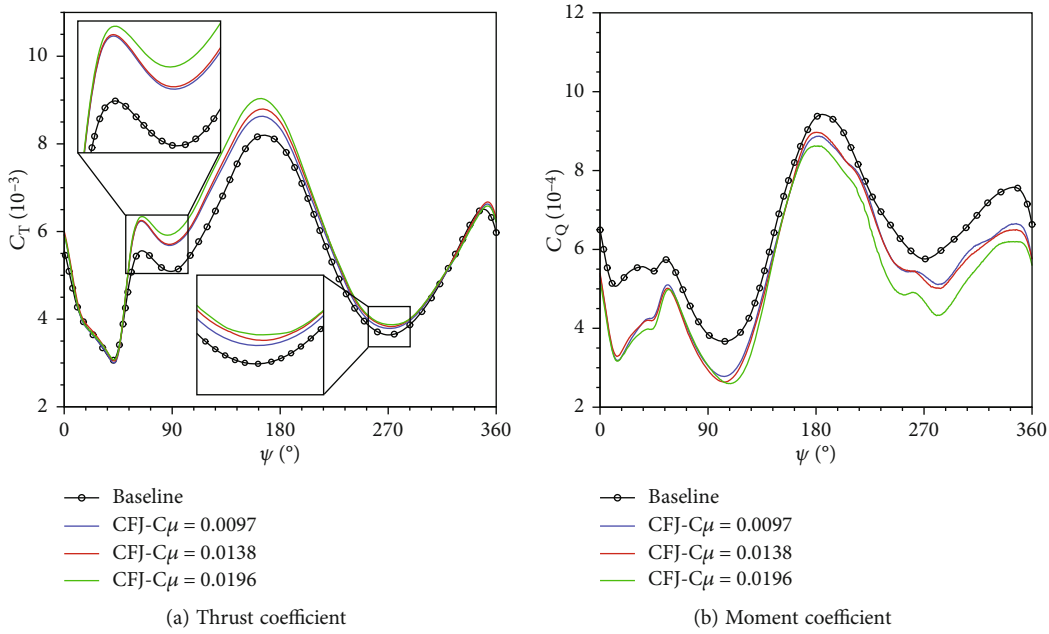

(a) Thrust coefficient (b) Moment coefficient

Figure 17: Thrust and moment coefficients vs. azimuth angle of the baseline rotor and CFJ-based rotors with different jet momentum coefficients.

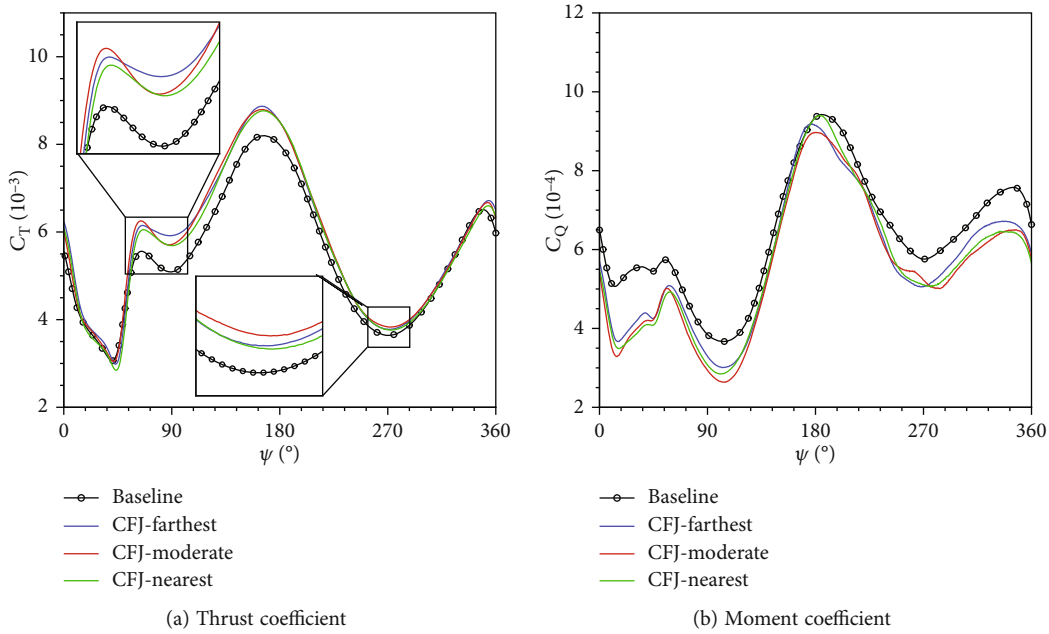

(a) Thrust coefficient (b) Moment coefficient

Figure 18: Thrust and moment coefficients vs. azimuth angle of the baseline rotor and CFJ-based rotors with different slot positions.

the three cases are farthest, moderate, and nearest. The other parameters for CFJ control are the same as those in Section 3.

Figure 18 shows the thrust and moment coefficients of the baseline rotor and CFJ-based rotors for slots in different positions along the blade. It can be seen that the thrust coefficient increased, and the moment coefficient decreased with CFJ control. The thrust coefficient increments for the farthest and nearest slots were close to that for the moderate slots, but the decrement of the moment coefficient for the farthest and nearest slots was smaller than that for the moderate slots. Hence, if the CFJ is too close to or too far from the rotor tip, the aerodynamic performance improvement will be weakened for the rotor.

4.3. Effect of CFJ Width. The effect of the width of the CFJ on the aerodynamic performance of the rotor is investigated in this section. The CFJ width was 0.15R, 0.2R, or 0.25R, respectively, and the symmetry plane was at $r = 0.85R$. The corresponding CFJ zones were 0.775R–0.925R, 0.75R

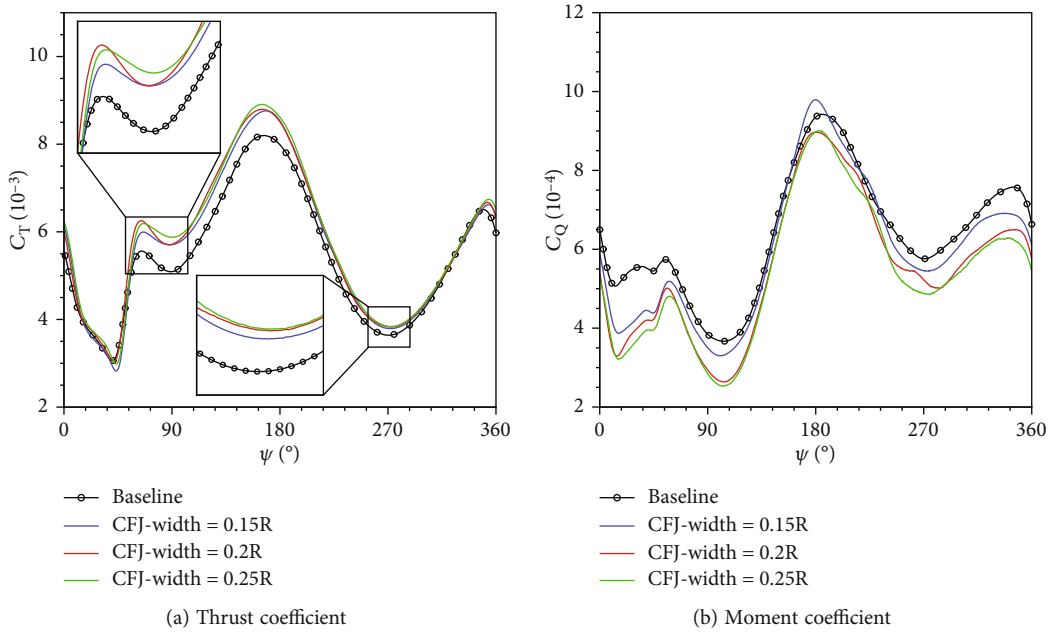

(a) Thrust coefficient (b) Moment coefficient

Figure 19: Thrust and moment coefficients vs. azimuth angle of the baseline rotor and CFJ-based rotors with different slot widths.

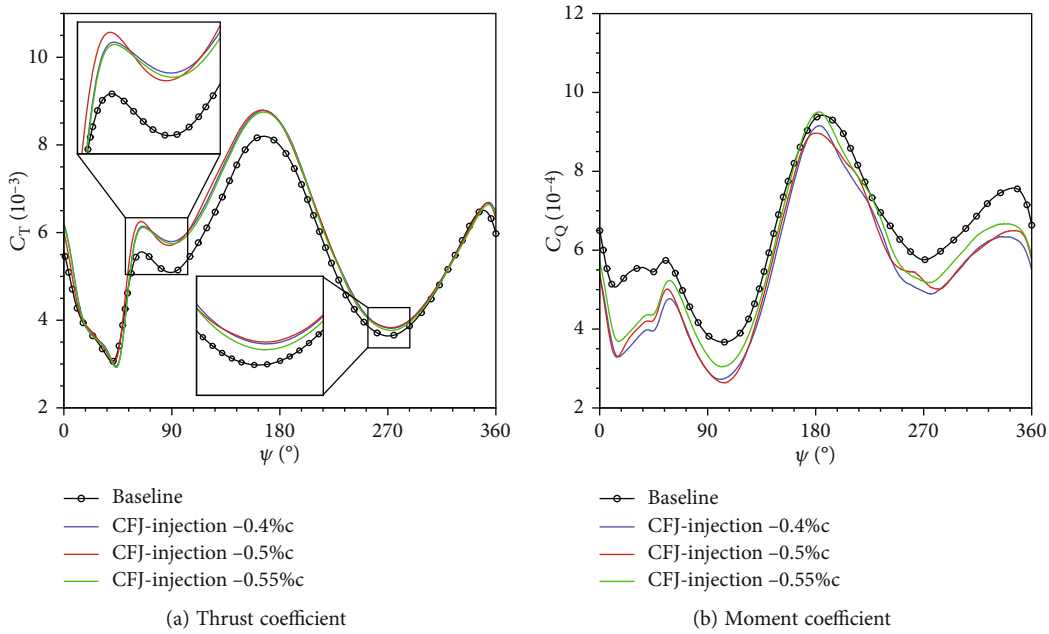

(a) Thrust coefficient (b) Moment coefficient

Figure 20: Thrust and moment coefficients vs. azimuth angle of the baseline rotor and CFJ-based rotors with different injection-slot heights.

–0.95R, and 0.725R–0.975R. The other parameters for the CFJ are the same as in Section 3.

The thrust and moment coefficients of the baseline rotor and CFJ-based rotors with different slot widths are presented in Figure 19. As shown, the greater the CFJ slot width, the greater the increment in the rotor thrust coefficient and the greater the decrement in the rotor moment coefficient compared to the baseline rotor. Thus, the aerodynamic performance improvement was enhanced for the rotor. However, the improvement for a width of 0.25R was not better than a width of 0.2R. The moment coefficient for a width of 0.15R was larger than that for the baseline rotor near the azimuth angle of 180°. Therefore, 0.2R is the best width for the CFJ.

4.4. Effect of CFJ Slot Height. The effect of the heights of the CFJ injection and suction slots on the aerodynamic performance of the rotor is investigated in this section. The CFJ control zone is 0.75R–0.95R. The CFJ momentum coefficient is the same as that in Section 3.

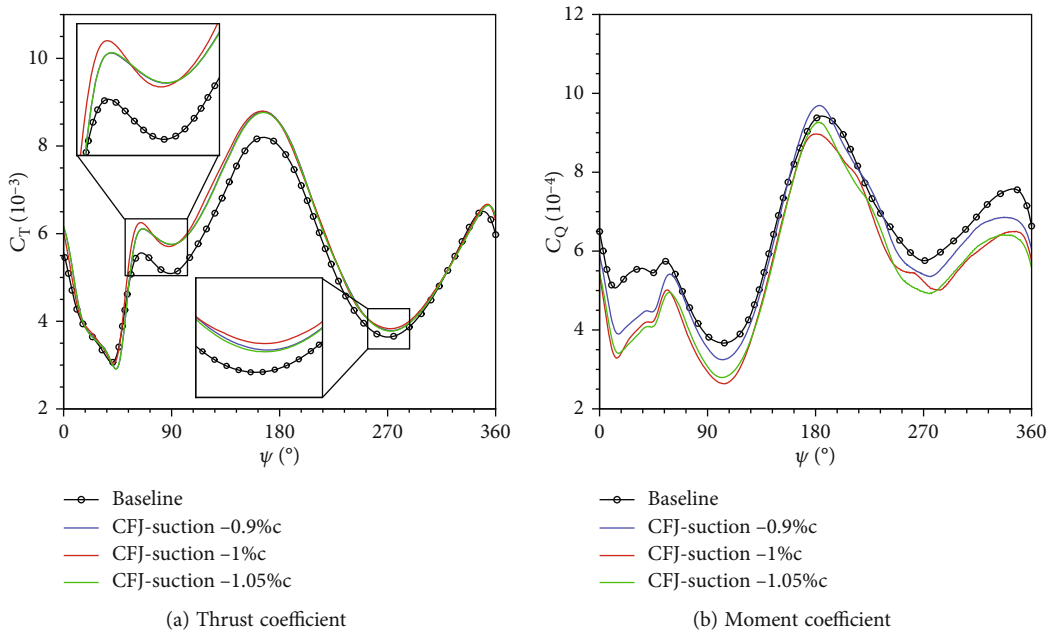

(a) Thrust coefficient (b) Moment coefficient

FIGURE 21: Thrust and moment coefficients vs. azimuth angle of the baseline rotor and CFJ-based rotors with different suction-slot heights.

First, the suction-slot height was fixed (1% of c), whereas the injection-slot height was 0.4% of c, 0.5% of c, or 0.55% of c. Figure 20 shows the thrust and moment coefficients of the baseline rotor and CFJ-based rotors with the injection slot at different heights. As the figure indicates, the injection-slot height had little effect on the increase of the rotor thrust coefficient. The reduction of the moment coefficient for a height of 0.4% of c was almost equal to that for a height of 0.5% of c. The effect was the worst when the injection-slot height was 0.55% of c, which demonstrates that the injection-slot height should not be too large.

Next, the injection-slot height was fixed (0.5% of c), and the suction-slot height was 0.9% of c, 1% of c, or 1.05% of c. Figure 21 shows the thrust and moment coefficients of the baseline rotor and CFJ-based rotors for different heights of the suction slot. It can be seen that the suction-slot height also had little effect on the increase of the rotor thrust coefficient. The reduction of the moment coefficient for a suction-slot height of 1% of c was almost equal to that for a suction-slot height of 1.05% of c. The effect was the worst when the suction-slot height was 0.9% of c, which demonstrates that the suction-slot height should not be too low.

5. Conclusions

In this study, an active control method based on CFJ is proposed to suppress the flow separation for improving the aerodynamic performance of a helicopter rotor. The effect of the CFJ parameters on improving the aerodynamic performance of a rotor was investigated. The main conclusions are as follows:

(1) With a CFJ at the rotor tip, the energy of the airflow near the wall of the rotor increased, which enhanced its ability to resist the adverse pressure gradient. The flow separation of the rotor was well suppressed, and the aerodynamic performance of the rotor was much improved. By investigating cases with different flight conditions, it was found that CFJ control has a generally excellent effect on improving the aerodynamic performance of a helicopter rotor

(2) Under forward-flight conditions, after applying CFJ control, the thrust coefficient of the rotor increased, and the moment coefficient decreased during the whole rotation period. The maximum increase of the thrust coefficient was about 5.5% on the advancing side, and the maximum increase was about 4.8% on the retreating side. The maximum reduction of the moment coefficient was about 26.8% on the advancing side, and the maximum reduction was about 16.0% on the retreating side. The equivalent lift-to-drag ratio of the rotor increased significantly, with a maximum increase of about 44.0%

(3) By solving and analyzing the rotor flow field with different CFJ parameters, some general conclusions were reached. The greater the jet momentum coefficient of the CFJ, the better the improvement of the aerodynamic performance of the rotor. If the CFJ is too close to or too far from the rotor tip, the improvement of the aerodynamic performance of the rotor will be weakened. The improvement of the aerodynamic performance of the rotor was best when the width of the CFJ was $0.2R$ and when the middle plane of the CFJ was at $r = 0.85R$. If the injection slot is too high and the suction slot is too low, the improvement of the aerodynamic performance of the rotor will be weakened

Data Availability

The data used to support the findings of this study are available from the corresponding author upon request.

Conflicts of Interest

The authors declare that there is no conflict of interest regarding the publication of this paper.

Acknowledgments

The work was supported by the National Natural Science Foundation of China under grant no. 12072305, National Key Laboratory of Science and Technology on Aerodynamic Design and Research under grant no. 614220121030202, Rotor Aerodynamics Key Laboratory under grant no. 2102RAL202101-2, Aeronautical Science Foundation of China under grant no. 20200057068001, Foreign Cooperation Projects of Fujian Province under grant no. 2020I0004, and Research Project under grant no. PZ2020016.

References

[1] W. Geissler, M. Raffel, G. Dietz, and H. Mai, "Helicopter aerodynamics with emphasis placed on dynamic stall," in *Wind Energy*, pp. 199–204, Springer, 2007.

[2] A. T. Conlisk, "Modern helicopter rotor aerodynamics," *Progress in Aerospace Sciences*, vol. 37, no. 5, pp. 419–476, 2001.

[3] Y. H. Yu, S. Lee, K. W. McAlister, C. Tung, and C. M. Wang, "Dynamic stall control for advanced rotorcraft application," *AIAA Journal*, vol. 33, no. 2, pp. 289–295, 1995.

[4] A. Brocklehurst and G. N. Barakos, "A review of helicopter rotor blade tip shapes," *Progress in Aerospace Sciences*, vol. 56, pp. 35–74, 2013.

[5] B. Wang, Q. Zhao, G. Zhao, and G. Xu, "Experimental research and numerical analysis on aerodynamic characteristics of rotors with improved CLOR blade-tip," *Acta Aeronautica et Astronautica Sinica*, vol. 34, no. 2, pp. 235–245, 2013.

[6] S. Chae, R. Yee, R. Yang, T. Aoyama, S. Jeong, and S. Obayashi, "Helicopter rotor shape optimization for the improvement of aeroacoustic performance in hover," *Journal of Aircraft*, vol. 47, no. 5, pp. 1770–1783, 2010.

[7] P. Doerffer, O. Szulc, and R. Bohning, "Shock wave smearing by passive control," *Journal of Thermal Science*, vol. 15, no. 1, pp. 43–47, 2006.

[8] P. Doerffer and O. Szulc, "Application of the passive control of shock wave to the reduction of high-speed impulsive noise," *International Journal of Engineering Systems Modelling & Simulation*, vol. 3, no. 1/2, pp. 64–73, 2011.

[9] H. Babinsky and J. K. Harvey, *Shock Wave-Boundary-Layer Interactions*, vol. 32, Cambridge University Press, 2011.

[10] A. Le Pape, M. Costes, F. Richez, G. Joubert, F. David, and J. M. Deluc, "Dynamic stall control using deployable leading-edge vortex generators," *AIAA Journal*, vol. 50, no. 10, pp. 2135–2145, 2012.

[11] B. Heine, K. Mulleners, G. Joubert, and M. Raffel, "Dynamic stall control by passive disturbance generators," *AIAA Journal*, vol. 51, no. 9, pp. 2086–2097, 2013.

[12] M. P. Kinzel, M. D. Maughmer, and E. P. N. Duque, "Numerical investigation on the aerodynamics of oscillating airfoils with deployable gurney flaps," *AIAA Journal*, vol. 48, no. 7, pp. 1457–1469, 2010.

[13] G. Gibertini, A. Zanotti, G. Droandi, F. Auteri, and G. Crosta, "Experimental investigation of a helicopter rotor with gurney flaps," *The Aeronautical Journal*, vol. 121, no. 1236, pp. 191–212, 2017.

[14] R. Pérez-Torró and J. W. Kim, "A large-eddy simulation on a deep-stalled aerofoil with a wavy leading edge," *Journal of Fluid Mechanics*, vol. 813, pp. 23–52, 2017.

[15] P. H. Ferreira, L. M. Brondani, J. R. Scarpari, F. L. Corrêa, A. A. de Paula, and R. G. da Silva, "Evaluation of wavy leading edge for rotary-wing applications," in *2018 Flow Control Conference*, p. 4255, Atlanta, Georgia, June 2018.

[16] A. Hassan, F. K. Straub, and K. W. Noonan, "Experimental/numerical evaluation of integral trailing edge flaps for helicopter rotor applications," *Journal of the American Helicopter Society*, vol. 50, no. 1, pp. 3–17, 2005.

[17] F. Samara and D. A. Johnson, "Deep dynamic stall and active aerodynamic modification on a S833 airfoil using pitching trailing edge flap," *Wind Engineering*, vol. 1, pp. 884–903, 2021.

[18] H. Y. Xu, S. L. Xing, Z. Y. Ye, and M. S. Ma, "Dynamic stall suppression for rotor airfoil based on inflatable leading edge technology," *Acta Aeronautica et Astronautica Sinica*, vol. 38, no. 6, pp. 86–98, 2017.

[19] S. L. Xing, H. Y. Xu, Z. Y. Ye, M. S. Ma, and Y. Xu, "Dynamic stall control using inflatable leading edge," *International Journal of Modern Physics B*, vol. 34, no. 14n16, p. 2040108, 2020.

[20] J. Niu, J. Lei, and T. Lu, "Numerical research on the effect of variable droop leading-edge on oscillating NACA 0012 airfoil dynamic stall," *Aerospace Science and Technology*, vol. 72, pp. 476–485, 2018.

[21] M. S. Chandrasekhara, P. B. Martin, and C. Tung, "Compressible dynamic stall control using a variable droop leading edge airfoil," *Journal of Aircraft*, vol. 41, no. 4, pp. 862–869, 2004.

[22] Q. J. Zhao, X. Chen, Y. Y. Ma, and G. Q. Zhao, "Investigations of synthetic jet control effects on helicopter rotor in forward flight based on the CFD method," *Aeronautical Journal*, vol. 122, no. 1253, pp. 1102–1122, 2018.

[23] Q. Zhao, Y. Ma, and G. Zhao, "Parametric analyses on dynamic stall control of rotor airfoil via synthetic jet," *Chinese Journal of Aeronautics*, vol. 30, no. 6, pp. 1818–1834, 2017.

[24] M. L. Post and T. C. Corke, "Separation control using plasma actuators: dynamic stall vortex control on oscillating airfoil," *AIAA Journal*, vol. 44, no. 12, pp. 3125–3135, 2006.

[25] A. J. Lombardi, P. O. Bowles, and T. C. Corke, "Closed-loop dynamic stall control using a plasma actuator," *AIAA Journal*, vol. 51, no. 5, pp. 1130–1141, 2013.

[26] T. C. Corke, P. O. Bowles, C. He, and E. H. Matlis, "Sensing and control of flow separation using plasma actuators," *Philosophical Transactions*, vol. 2011, no. 369, pp. 1459–1475, 1940.

[27] G. Zha and W. Gao, "Analysis of jet effects on co-flow jet airfoil performance with integrated propulsion system," in *44th AIAA Aerospace Sciences Meeting and Exhibit*, p. 102, Reno, Nevada, 2006.

[28] G. C. Zha, B. F. Carroll, C. D. Paxton, C. A. Conley, and A. Wells, "High-performance airfoil using coflow jet flow control," *AIAA Journal*, vol. 45, no. 8, pp. 2087–2090, 2007.

[29] G. Zha, W. Gao, and C. D. Paxton, "Jet effects on coflow jet airfoil performance," *AIAA Journal*, vol. 45, no. 6, pp. 1222–1231, 2007.

[30] R. Englar, "Circulation control pneumatic aerodynamics: blown force and moment augmentation and modification - past, present and future," in *Fluids 2000 Conference and Exhibit*, Denver, CO, USA, 2000.

[31] B. Y. Min, W. Lee, R. Englar, and L. N. Sankar, "Numerical investigation of circulation control airfoils," *Journal of Aircraft*, vol. 46, no. 4, pp. 1403–1410, 2009.

[32] B. Wang, B. Haddoukessouni, J. Levy, and G. C. Zha, "Numerical investigations of injection-slot-size effect on the performance of coflow jet airfoils," *Journal of Aircraft*, vol. 45, no. 6, pp. 2084–2091, 2008.

[33] A. J. Wells, *Experimental Investigation of an Airfoil with co-Flow Jet Flow Control*, University of Florida, 2005.

[34] A. M. Lefebvre, *Investigation of Co-Flow Jet Flow Control and Its Applications*, University of Miami, 2015.

[35] Y. C. Yang and G. C. Zha, "Numerical investigation of performance improvement of the co-flow jet electric airplane," in *2018 Applied Aerodynamics Conference*, Atlanta, Georgia, 2018.

[36] M. G. Fernandez, J. Hoffmann, and G. Zha, "Transonic supercritical airfoil enhancement by coflow jet downstream of normal shock," in *2018 Flow Control Conference*, Atlanta, Georgia, 2018.

[37] Z. Liu and G. Zha, "Transonic airfoil performance enhancement using co-flow jet active flow control," in *AIAA Flow Control Conference*, Washington, D.C., 2016.

[38] X. D. Yang, W. R. Jiang, and S. L. Zhang, "Analysis of co-flow jet effect on dynamic stall characteristics applying to rotor airfoils," *IOP Conference Series Materials Science and Engineering*, vol. 491, 2019.

[39] H. Y. Xu, C. L. Qiao, and Z. Y. Ye, "Dynamic stall control on the wind turbine airfoil via a co-flow jet," *Energies*, vol. 9, no. 6, p. 429, 2016.

[40] J. Q. Liu, R. Q. Chen, R. F. Qiu, Y. You, and W. Zhang, "Study on dynamic stall control of rotor airfoil based on coflow jet," *International Journal of Aerospace Engineering*, vol. 2020, 15 pages, 2020.

[41] J. Q. Liu, R. Q. Chen, Y. C. You, and Z. Y. Shi, "Numerical investigation of dynamic stall suppression of rotor airfoil via improved co-flow jet," *Chinese Journal of Aeronautics*, vol. 35, no. 3, pp. 169–184, 2022.

[42] J. Blazek, *Computational Fluid Dynamics: Principles and Applications*, Butterworth-Heinemann, 2015.

[43] P. L. Roe, "Approximate Riemann solvers, parameter vectors, and difference schemes," *Journal of Computational Physics*, vol. 43, no. 2, pp. 357–372, 1981.

[44] A. Jameson, "Time dependent calculations using multigrid, with applications to unsteady flows past airfoils and wings," in *10th Computational Fluid Dynamics Conference*, Honolulu, HI, USA, 1991.

[45] F. R. Menter, "Two-equation eddy-viscosity turbulence models for engineering applications," *AIAA Journal*, vol. 32, no. 8, pp. 1598–1605, 1994.

[46] J. A. Benek, P. G. Buning, and J. L. Steger, "A 3-D chimera grid embedding technique," in *7th Computational Physics Conference*, Cincinnati, OH, U.S.A., 1985.

[47] J. Ahmad and E. P. Duque, "Helicopter rotor blade computation in unsteady flows using moving overset grids," *Journal of Aircraft*, vol. 33, no. 1, pp. 54–60, 1996.

[48] R. Noack, "SUGGAR: a general capability for moving body overset grid assembly," in *17th AIAA Computational Fluid Dynamics Conference*, Toronto, Ontario, Canada, 2005.

[49] Y. H. Yu, C. Tung, J. Gallman et al., "Aerodynamics and acoustics of rotor blade-vortex interactions," *Journal of Aircraft*, vol. 32, no. 5, pp. 970–977, 1995.

[50] A. Lefebvre, B. Dano, W. B. Bartow, M. Difronzo, and G. C. Zha, "Performance and energy expenditure of coflow jet airfoil with variation of Mach number," *Journal of Aircraft*, vol. 53, no. 6, pp. 1757–1767, 2016.

[51] F. X. Caradonna and C. Tung, *Experimental and Analytical Studies of a Model Helicopter Rotor in Hover*, European Rotorcraft and Powered Lift Aircraft Forum, 1981.